# *N*-Ethyl-*N*-propylpyrrolidinium Bis(fluorosulfonyl)amide Ionic Liquid Electrolytes for Sodium Secondary Batteries: Effects of Na Ion Concentration

*Huan Yang[1], Jinkwang Hwang[1], Yushen Wang[1], Kazuhiko Matsumoto[1,2*], Rika Hagiwara[1,2]*

*[1]Graduate School of Energy Science, Kyoto University, Yoshida-honmachi, Sakyo-ku, Kyoto 606-8501, Japan*

*[2]Unit of Elements Strategy Initiative for Catalysts & Batteries (ESICB), Kyoto University, Katsura, Kyoto 615-8510, Japan*

*Corresponding author: Kazuhiko Matsumoto
E-mail: k-matsumoto@energy.kyoto-u.ac.jp

ABSTRACT

A hybrid inorganic-organic ionic liquid based on sodium bis(fluorosulfonyl)amide (Na[FSA]) and [*N*-ethyl-*N*-methylpyrrolidinium][FSA] ([$C_2C_1$pyrr][FSA]) is investigated as an electrolyte for sodium secondary battery operation over an extended temperature and $Na^+$ ion fraction ranges. The phase diagram of the system reveals a wide liquid-phase temperature range at Na[FSA] mole fractions ranging from 0.3 to 0.7 near room temperature, where the 0.7 mole fraction equates to a molar concentration of 5.42 mol $L^{-1}$. The viscosity and molar ionic conductivity are consistent with the fractional Walden rule, and the temperature dependence of these quantities obeys the Vogel−Tammann−Fulcher equation. The optimal Na[FSA] content of the ionic liquid occurs at mole fractions between 0.3 and 0.7 based on the sodium metal deposition/dissolution behavior and the rate and cycle properties of a NASICON-type cathode, $Na_3V_2(PO_4)_3$/C (NVPC). The greatest cycle efficiency, $\varepsilon_{cycle,}$ of Na metal deposition/dissolution is observed at $x$(Na[FSA]) = 0.6 ($\varepsilon_{cycle}$ = 93.3%). Although Na/NVPC half-cell tests indicate a maximum rate and cycle performance at $x$(Na[FSA]) = 0.6 (83.5% retention at 100 C (11700 mA $g^{-1}$) and 80% retention after 4000 cycles at 2 C (234 mA $g^{-1}$), NVPC/NVPC symmetric cell tests indicate that the greater Na[FSA] fraction provides better rate performance and that half-cell tests with a Na metal electrode do not provide reliable data for the target electrode/electrolyte system.

## 1. INTRODUCTION

Ionic liquids (ILs) contain only ionic species and are characterized by unique properties such as non-flammability, non-volatility, high thermal and electrochemical stability, a wide electrochemical window, and a wide liquid temperature range that includes room temperature.[1] These properties allow ILs to be used as electrolytes in energy-related devices such as secondary batteries, electrochemical capacitors, fuel cells, and dye-sensitized solar cells.[2-8] Ongoing research is directed towards alternative energy conversion and storage solutions to confront the existing energy crisis.[9] Organic-solvent electrolytes are used in almost all current Li/Na secondary batteries despite their volatility and flammability, which carries the significant risk of fire or explosion. The suitability of IL electrolytes in such devices has been discussed frequently over the past decade.[10-13] ILs are now considered to be safer alternatives to conventional organic electrolytes and to be compatible with operation over a wide temperature range. This property facilitates the intermediate temperature operation of secondary batteries utilizing waste heat and improves battery performance by enhancing ion transport and electrode reaction rates.[14-15]

Bis(trifluoromethylsulfonyl)amide ($TFSA^-$) and bis(fluorosulfonyl)amide ($FSA^-$) are typical IL anions that possess high chemical and electrochemical stability and form salts with low melting points.[16-17] Many ILs based on $TFSA^-$ and $FSA^-$ have been reported to date.[18-24] $FSA^-$ forms significantly less viscous ILs than $TFSA^-$ and other chemically inert anions.[25-29] A low viscosity provides the fluidity needed to operate energy storage devices at room-to-intermediate temperatures.[30-31] The cathodic stability

of $FSA^-$ also enables its use as a negative electrode material in Li batteries.[32-35] Some reports claim that $FSA^-$-based ILs form a robust solid-electrolyte interphase (SEI) on $Li^0$, which suppresses dendrite formation in Li batteries.[27, 32-34, 36]

Lithium secondary batteries has been widely studied and dominate the global secondary battery market, but sodium battery energy storage systems (ESS) is expected to precede Li-ion battery in a near future with high natural abundance, low cost, and even distribution of lithium resources.[37] In particular, sodium secondary batteries are emerging energy storage devices in large scale applications[38] owing to the greater availability of Na relative to Li resources.[39] The safety advantages of ILs are evident due to their unique properties. Some physical and electrochemical investigations have described the potential of Na[FSA]–[$C_3C_1$pyrr][FSA] ($C_3C_1$pyrr: *N*-methyl-*N*-propylpyrrolidinium) and Na[FSA]–[$C_2C_1$im][FSA] ($C_2C_1$im: 1-ethyl-3-methylimidazolium) as IL electrolytes in Na secondary batteries.[40-44] These studies have determined that the Na mole fraction is an important factor affecting battery operation and that the optimal Na fraction depends on temperature and the electrochemical reaction.[42-43, 45] The rate capability of positive electrode materials is more difficult to evaluate, because polarization of the Na counter electrode in a two-electrode cell is significant even at elevated temperatures.[46-47] Evaluation of electrode materials covering a wide range of Na compositions is required to establish the optimal Na salt concentration in practical cells. This need prompted us to investigate and characterize new IL electrolytes based on $C_2C_1pyrr^+$ and $FSA^-$. It is notable that organic ionic plastic crystals are also attractive materials possessing a plastic crystalline phase

observed over a wide temperature range, which is advantageous for its applications in electrochemical devices.[44] Organic ionic plastic crystal phase often appears along with ILs, especially in the case of onium salts with a relatively spherical cation (e.g. $C_2C_1pyrr^+$).[48] The thermal and physical properties of the Na[FSA]–[$C_2C_1$pyrr][FSA] system are reported in this study. A Na[FSA]–[$C_2C_1$pyrr][FSA] phase diagram constructed from differential scanning calorimetry (DSC) results is used to establish the optimal temperature range of the electrolyte. In addition to the basic physicochemical and electrochemical properties of Na[FSA]–[$C_2C_1$pyrr][FSA], we have investigated the Na metal deposition/dissolution behavior and the effects of *x*(Na[FSA]) on the rate and cycle performance of $Na_3V_2(PO_4)_3$/C (NVPC, "C" denotes carbon coat), which is a widely studied positive electrode material in sodium secondary batteries.[49-50] A NVPC/NVPC symmetric cell is also evaluated to address concerns regarding the effect of the Na metal counter electrode on cell performance.

## 2. EXPERIMENTAL SECTION

### 2.1. Material Synthesis.

Moisture- and air-sensitive materials were handled in a glove box (Miwa Manufacturing Co., Ltd.) under dry deoxygenated Ar gas. The dew point (below 193 K) and oxygen content (below 1 ppm, Oxygen Analyzer DF-150E, General Electric Company) were monitored during the experiment. Electrode materials and reagents were weighed using an electric balance (CPA225D, Sartorius; WMC25-SH, Mettler Toledo) in the glove box. Na[FSA] (Mitsubishi Materials Electronic Chemicals Co.,

Ltd., purity >99%) was dried under vacuum for 24 h at 353 K prior to use. $[C_2C_1pyrr][FSA]$ was synthesized from K[FSA] (Materials Electronic Chemicals Co., Ltd., purity >99%) and $[C_2C_1pyrr]Br$ (Sigma-Aldrich, purity 99%) by a metathesis reaction according to a previous report[48] (see Supporting Information for details). The water content of $[C_2C_1pyrr][FSA]$ was < 30 ppm by Karl-Fisher titration. The K and Br impurity contents were below their detectable limits ($K^+$ < 63 ppm, $Br^-$ < 1 ppm) by X-ray fluorescence (XRF) spectroscopy. Powdery Na[FSA] and waxy $[C_2C_1pyrr][FSA]$ were weighed to the desired molar ratio and mixed together. The mixture was completely dissolved in super-dry acetonitrile (Wako Pure Chemical Industries, purity 99.5%, $H_2O$ <10 ppm). The solvent was removed under vacuum at 333 K to obtain a homogeneous sample. All samples were stored in the glove box at room temperature.

2.2. Physical and Thermal Characterization

Phase transition temperatures were determined by DSC (DSC-8230 Thermo Plus EVO II Series, Rigaku Corp.) at a scan rate of 5 K $min^{-1}$ under a dry Ar atmosphere. The thermal stability was measured by thermogravimetric (TG) analysis (STA2500 Regulus, NETZSCH) at a scan rate of 5 K $min^{-1}$ under a dry Ar atmosphere. DSC samples were sealed in an Al pan, and TG samples were loaded in an Al pan in the glove box. Viscosities were measured with an electromagnetically spinning viscometer EMS-100 (Kyoto Electronics Manufacturing Co., Ltd.). Samples were sealed in glass tubes with a spherical Al probe in the glove box. The ionic conductivity was measured by an AC impedance technique using a 3532-80 impedance analyzer (Hioki E.E. Corp.).

Samples were sealed in a T-shaped cell with two stainless steel electrodes in the glove box and placed in a temperature-controlled thermostatic chamber (SU-242, ESPEC). The density was measured with an oscillating U-tube density meter (DMA 4500 M, Anton Paar GmbH). Tetradecane (Wako Pure Chemical Industries, purity >99%) was used as a standard due to its stability upon heating. The water content was measured by Karl-Fischer titration (899 Coulometer, Metrohm). Some impurity contents were measured by energy dispersive X-ray fluorescence spectrometry (Rigaku, EDX-300) at a voltage of 50 kV and current of 2 mA. Samples were sealed in a plastic cell with a proline window and placed in a He flow during measurements.

2.3. Electrochemical Characterization.

Charge/discharge behavior was measured using a HJ1001SD8 device (Hokuto Denko) following storage of the cells at a target temperature in the thermostatic chamber for at least 3 h. Electrochemical stability was examined using a VSP-300 electrochemical system (Bio-Logic) using a two-electrode coin cell comprising a Pt- or Al-plate working electrode (13-mm diameter, 0.20-mm thickness) and a Na metal counter electrode. Cyclic voltammetry was performed at 5 mV $s^{-1}$ at 298 and 363 K. Sodium deposition/dissolution was performed at a current density of 0.1 mA $cm^{-2}$ in Na[FSA]-[$C_2C_1$pyrr][FSA] electrolyte with $x$(Na[FSA]) = 0.3–0.7 at 298 and 363 K using Al working and Na counter electrodes. 1.0 C $cm^{-2}$ Na metal was deposited on the Al substrate, and 0.2 C $cm^{-2}$ Na dissolution/deposition was repeated until the electrode potential reached 0.5 V vs. $Na^+$/Na during dissolution. The average cycle efficiency of

Na deposition/dissolution ($\varepsilon_{cycle}$) is described by Eq. (1):

$$\varepsilon_{cycle} = N_{eff} \cdot Q_{cycle} / (Q_{ex} + N_{eff} \cdot Q_{cycle}) \quad (1)$$

where $N_{eff}$ is the number of cycles until the electrode potential reaches 0.5 V vs. $Na^+/Na$, $Q_{cycle}$ is the electric charge for Na deposition/dissolution (0.2 C $cm^{-2}$), and $Q_{ex}$ is the extra amount of electricity theoretically unused (0.8 C $cm^{-2}$). The cathode in the half-cell for rate and cycle tests was the carbon-coated $Na_3V_2(PO_4)_3$ material ($Na_3V_2(PO_4)_3$:Super C65:PTFE=80:15:5, where Super C65 is a conductive additive and PTFE is a binder) reported in previous work.[14] NVPC served as the anode and cathode in the symmetric cell used to determine the influence of the anode on the half-cell performance. The theoretical capacities of NVPC serving as a positive or negative electrode via the $V^{3+}/V^{4+}$ and $V^{3+}/V^{2+}$ redox reactions are unequal (117.6 mAh $g^{-1}$ and 55.0 mAh $g^{-1}$, respectively). Thus, a positive-to-negative mass loading ratio of 1:2.5 was used maintain capacity at the negative terminal. Mass loadings of 1.2 and 3.0 mg $cm^{-2}$ were used for the positive and negative electrodes, respectively (0.785 $cm^2$ area for both electrodes).

## 3. RESULTS AND DISCUSSION

### 3.1. Thermal Behavior

The thermal stability of Na[FSA]–[$C_2C_1$pyrr][FSA] was investigated by TG (see Table S1 and Figure S2). The [$C_2C_1$pyrr][FSA] single salt exhibits a thermal

decomposition temperature of 578 K based on a 5 wt% loss, which is similar to the reported value (576 K).[48] The 1:1 mixture exhibits a small decrease in weight near 430 K, which is followed by a small step loss at 485 K and a major decrease at 530 K (Figure S2). The mixture has a lower decomposition temperature than the single salt, which accords with the accelerated decomposition of $[C_2C_1pyrr][FSA]$ in the presence of $Na^+$ that is attributed to the lower decomposition temperature of neat Na[FSA].[51]

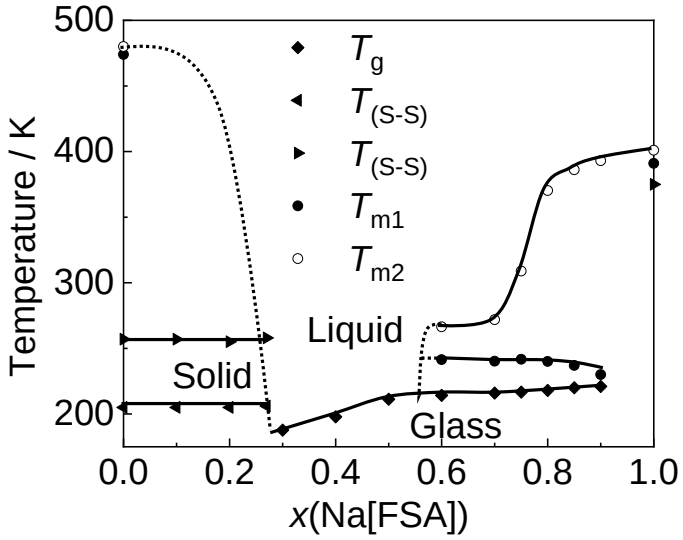


**Figure 1.** Phase diagram of the Na[FSA]-$[C_2C_1pyrr][FSA]$ system. $T_{m1}$: onset temperature of melting, $T_{m2}$: end temperature of melting, $T_{s-s}$: solid–solid transition temperature, and $T_g$: glass transition temperature. The DSC curves and transition temperatures are summarized in Figure S3 and Table S2, respectively.

The phase behavior of Na[FSA]–$[C_2C_1pyrr][FSA]$ at $x$(Na[FSA]) = 0–1.0 was investigated by DSC (Figure S3 and Table S2). Figure 1 shows the phase diagram of the Na[FSA]–$[C_2C_1pyrr][FSA]$ system. The upper limit of DSC measurements was 393 K except for neat $[C_2C_1pyrr][FSA]$, because decomposition of the 1:1 mixture begins

at approximately 400 K according to TG analysis. Thus, $T_m$ cannot be determined at $x$(Na[FSA]) = 0.10–0.25, and a dashed line is drawn to illustrate the behavior in this region. The DSC curve of the [$C_2C_1$pyrr][FSA] single salt exhibits solid-solid phase transitions at 205 and 257 K upon heating, followed by melting at 478 K. This behavior agrees with a previous report.[48] Samples with $x$(Na[FSA]) = 0.1−0.3 are sticky and waxy. These are considered to be mixtures of liquid and a plastic crystalline material based on the fact that neat [$C_2C_1$pyrr][FSA] forms a plastic crystal phase between 255 and 478 K.[48] No crystallization occurs at $x$(Na[FSA]) = 0.3−0.5, and only a glass transition is observed during DSC measurements. The glass transition temperature increases with increasing $x$(Na[FSA]) at $x$(Na[FSA]) = 0.3−0.9. As previously proposed for ILs,[52] the glass transition temperature correlates with ionic motion and conductivity. This trend is observed in the present case, where ionic conductivity decreases with increasing $x$(Na[FSA]) (see below for details). A pair of transition peaks appear near 250 K at $x$(Na[FSA]) = 0.6 and continue to be observed at $x$(Na[FSA]) = 0.7−0.9. Similar behavior has been reported in the high $x$(Na[FSA]) range of the Na[FSA]–[$C_3C_1$pyrr][FSA] system[53] and has been interpreted to indicate the existence of a metastable phase[40]. The onset and end temperatures of melting, $T_{m1}'$ and $T_{m2}'$, for the metastable phase are listed in Table S2. The $T_{m1}'$ is greater than $T_{m1}$ at $x$(Na[FSA]) = 0.6−0.9. The present case suggests that the metastable phase is caused by crystallization of one of the Na[FSA] polymorphs, because analogous metastable phases are observed at similar temperatures regardless of the organic cation structure, and a variety of polymorphic behavior is known for FSA salts[53]. The remaining Na[FSA] in the solid-

liquid mixture at $x$(Na[FSA]) = 0.7−0.9 melts above 305 K. According to this phase diagram, a broad liquid temperature range from low to intermediate temperatures is achieved at $0.3 \leq x(\text{Na[FSA]}) \leq 0.7$. Significantly, the liquid phase observed from room to intermediate temperature at $x$(Na[FSA]) > 0.5, which has not been in encountered in previous studies of Na[FSA]–[$C_3C_1$pyrr][FSA] and Na[FSA]–[$C_2C_1$im][FSA] systems,[40, 43] enables us to examine the effects of high $Na^+$ concentrations on electrode behavior.

3.2. Viscosity, Ionic Conductivity, and Density.

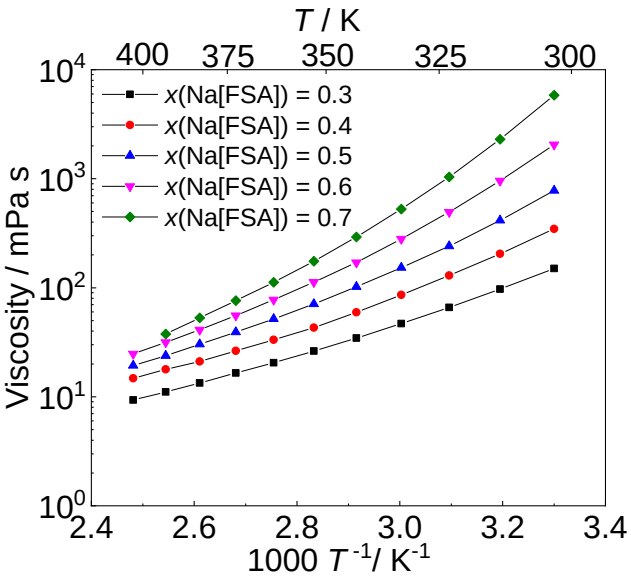


**Figure 2.** Temperature dependence of Na[FSA]–[$C_2C_1$pyrr][FSA] viscosity at $x$(Na[FSA]) = 0.30–0.70.

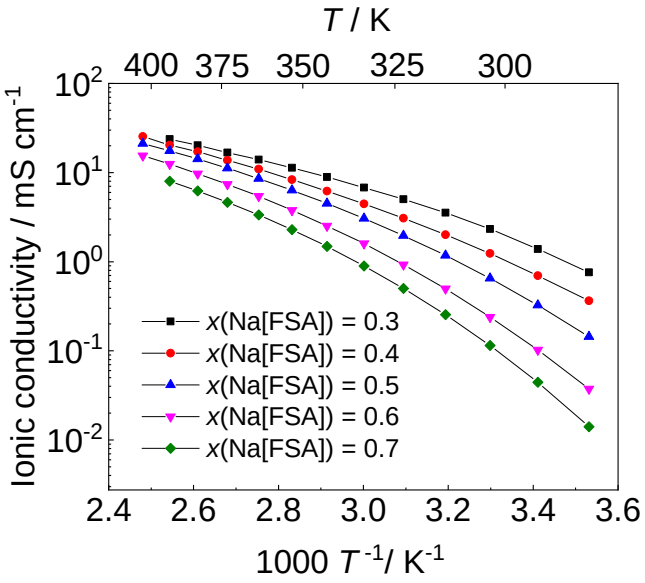


**Figure 3.** Temperature dependence of Na[FSA]–[$C_2C_1$pyrr][FSA] ionic conductivity at *x*(Na[FSA]) = 0.30–0.70.

Temperature dependences of the viscosity, ionic conductivity, and density of the Na[FSA]−[$C_2C_1$pyrr][FSA] system are shown in Figures 2, 3, and 4, respectively. The changes in viscosity and ionic conductivity exhibit concave and convex behavior, respectively, and fit well with the Vogel-Tammann-Fulcher (VTF) equation as do many conventional ILs.[31, 54-55] Tables S3–S6 in the Supporting Information contain experimental data and VTF fitting parameters for viscosity and ionic conductivity. The ionic conductivity at Na[FSA] = 0.3 is 1.39 mS $cm^{-1}$ at 298 K and increases to 23.72 mS $cm^{-1}$ at 363 K. These values are similar to those of Na[FSA]–[$C_3C_1$pyrr][FSA] at the same composition and temperature (e.g., 1.9 mS $cm^{-1}$ at *x*(Na[FSA]) = 0.3 at 298 K),[43] whereas the imidazolium-based Na[FSA]–[$C_2C_1$im][FSA] system yields higher ionic conductivities (5.55 mS $cm^{-1}$ at *x*(Na[FSA]) = 0.3 at 298 K).[40] The difference results from the intrinsic difference in fluidity between imidazolium- and

pyrrolidinium-based ILs (8.0 and 16.6 mS $cm^{-1}$ for $[C_3C_1pyrr][FSA]$ and $[C_2C_1im][FSA]$, respectively). The general trends in viscosity and ionic conductivity agree with the behavior of previous IL systems. The viscosity increases and ionic conductivity decreases with increasing $x$(Na[FSA]) and decreasing temperature in accord with the fractional Walden rule. Figure S4 contains a Walden plot for the system.

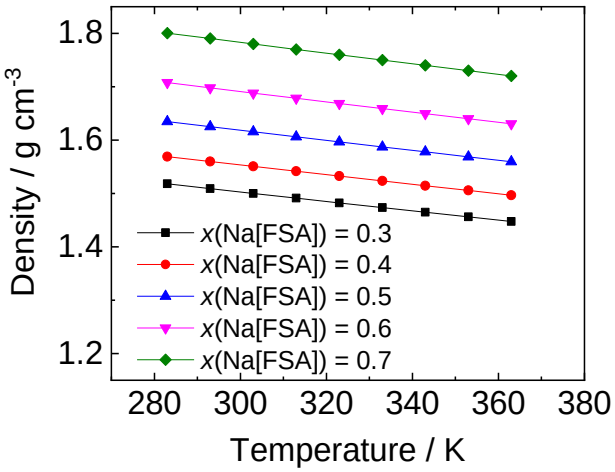


**Figure 4.** Temperature dependence of Na[FSA]–$[C_2C_1pyrr][FSA]$ density at $x$(Na[FSA]) = 0.30–0.70.

The density of Na[FSA]–$[C_2C_1pyrr][FSA]$ is linearly dependent on temperature from 283 to 363 K (Figure 4). The density is fit to Eq. 2 as illustrated by the data in Table S7:

$$\rho = AT + B \qquad (2)$$

Density decreases with increasing temperature and decreasing $x$(Na[FSA]). The molar concentration of Na[FSA] at different $x$(Na[FSA]) values in the Na[FSA]–$[C_2C_1pyrr][FSA]$ system is calculated from the density and formula weights

summarized (Table S8). The Na[FSA] molar concentration at $x$(Na[FSA]) = 0.7 reaches 5.42 mol $L^{-1}$ at 298 K and 5.22 mol $L^{-1}$ at 363 K. A large Na[FSA] concentration is advantageous in that it improves electrochemical performance by increasing the supply of $Na^+$ ions to the electrode surface, although the viscosity increases.

### 3.3. Electrochemical Stability and Cycling Efficiency of Na Metal Deposition/Dissolution.

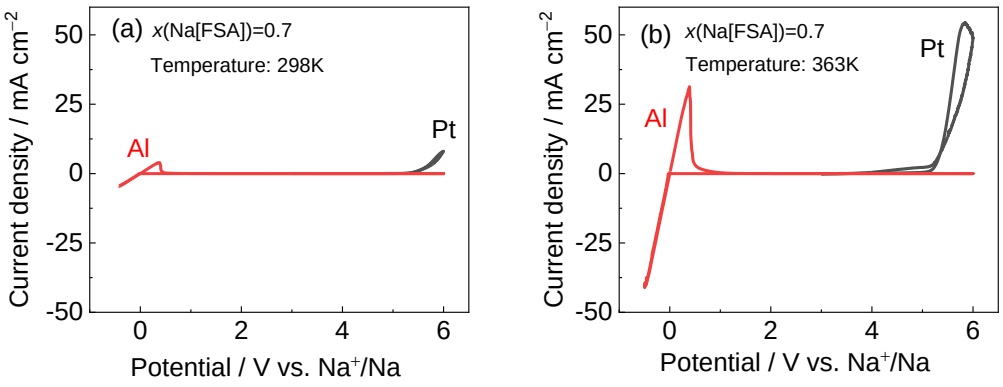


**Figure 5.** Combined cyclic voltammograms of Al (positive and negative potentials) and Pt (positive positive) plate electrodes in Na[FSA]-[$C_2C_1$pyrr][FSA] ($x$(Na[FSA]) = 0.7) at (a) 298 and (b) 363K. Scan rate: 5 mV $s^{-1}$. See Figure S7 for cyclic voltammograms of $x$(Na[FSA]) = 0.3–0.6 at 298 and 363 K.

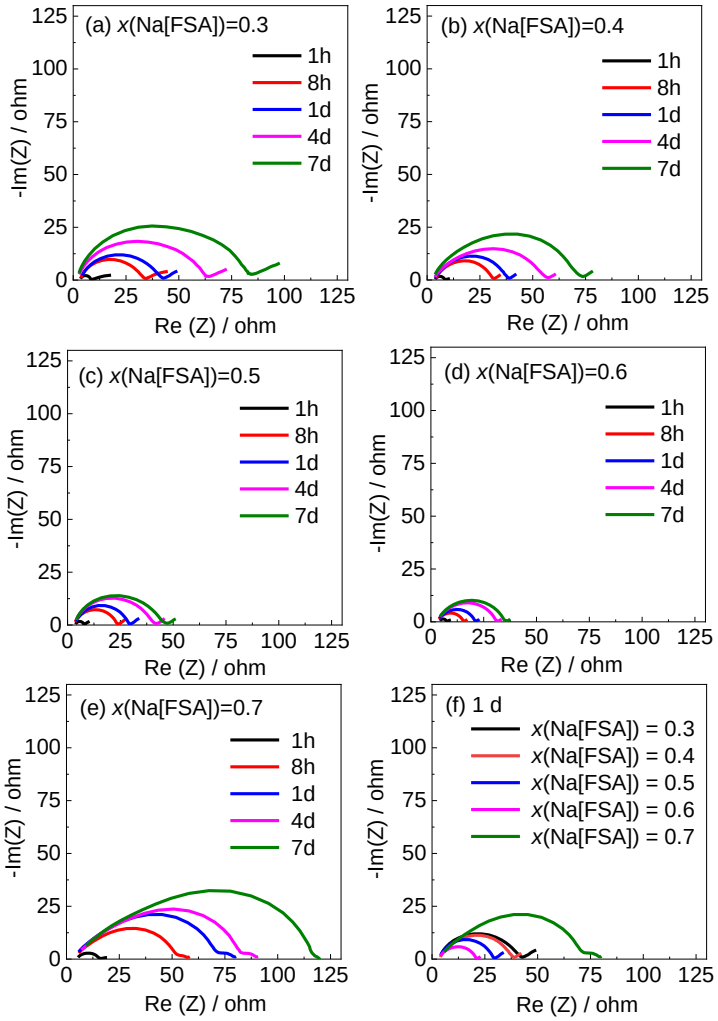


**Figure 6.** Nyquist plots (a–e) of Na/Na symmetric cells in Na[FSA]-[$C_2C_1$pyrr][FSA] ($x$(Na[FSA]) = 0.3–0.7) at 363 K over 7 d. Nyquist plots (f) at $x$(Na[FSA]) = 0.3–0.7 after 1 d. AC perturbation: 10 mV, frequency range: 10 mHz to 100 kHz.

Figure 5 shows combined cyclic voltammograms of Al (at positive and negative potentials) and Pt (positive potentials) plate electrodes in Na[FSA]-[$C_2C_1$pyrr][FSA] ($x$(Na[FSA])= 0.7) at 298 and 363 K in a two-electrode cell with a Na metal counter electrode. At negative potentials, the cathodic and anodic currents near 0 V vs. $Na^+$/Na at the Al electrode correspond to electrodeposition and electrodissolution, respectively, of Na metal. Figure S7 shows that the slopes of the cyclic voltammetric traces of Na

deposition and dissolution increase with increasing $x$(Na[FSA]) reflect a decrease in the charge-transfer resistance, $R_{ct}$, of the electrode reaction. This behavior is confirmed in Figure 6 by the electrochemical impedance spectroscopy (EIS) results for symmetric Na/Na cells, where the radius of the semicircles in the Nyquist plots decreases with increasing $x$(Na[FSA]). The results are not influenced by the bulk resistance, which is small and does not significantly change as a function of $x$(Na[FSA]). The charge transfer resistance, $R_{ct}$, semicircles decrease in radius as the Na[FSA] mole fraction increases from 0.3 to 0.6 and increase again at $x$(Na[FSA]) = 0.7. This behavior indicates that the supply of $Na^+$ is sufficient to sustain formation of a robust SEI layer to protect the IL from decomposition at the Na counter electrode. Figure 5 also shows that the anodic limit, where irreversible decomposition of the IL electrolyte occurs, is beyond 5.0 V at the Pt electrode. This result confirms the suitability of the system as a state-of-the-art positive electrode at 298 and 363 K.

Figure 7 displays the voltage profiles during Na metal deposition/dissolution in Na[FSA]-[$C_2C_1$pyrr][FSA] with $x$(Na[FSA]) = 0.3–0.7 at 298 and 363 K. The $\varepsilon_{cycle}$ was evaluated according to Eq. (1). Figure 8 shows the effects of temperature and Na[FSA] mole fraction on $\varepsilon_{cycle}$. An increase in temperature improves $\varepsilon_{cycle}$ at all $x$(Na[FSA]) values.

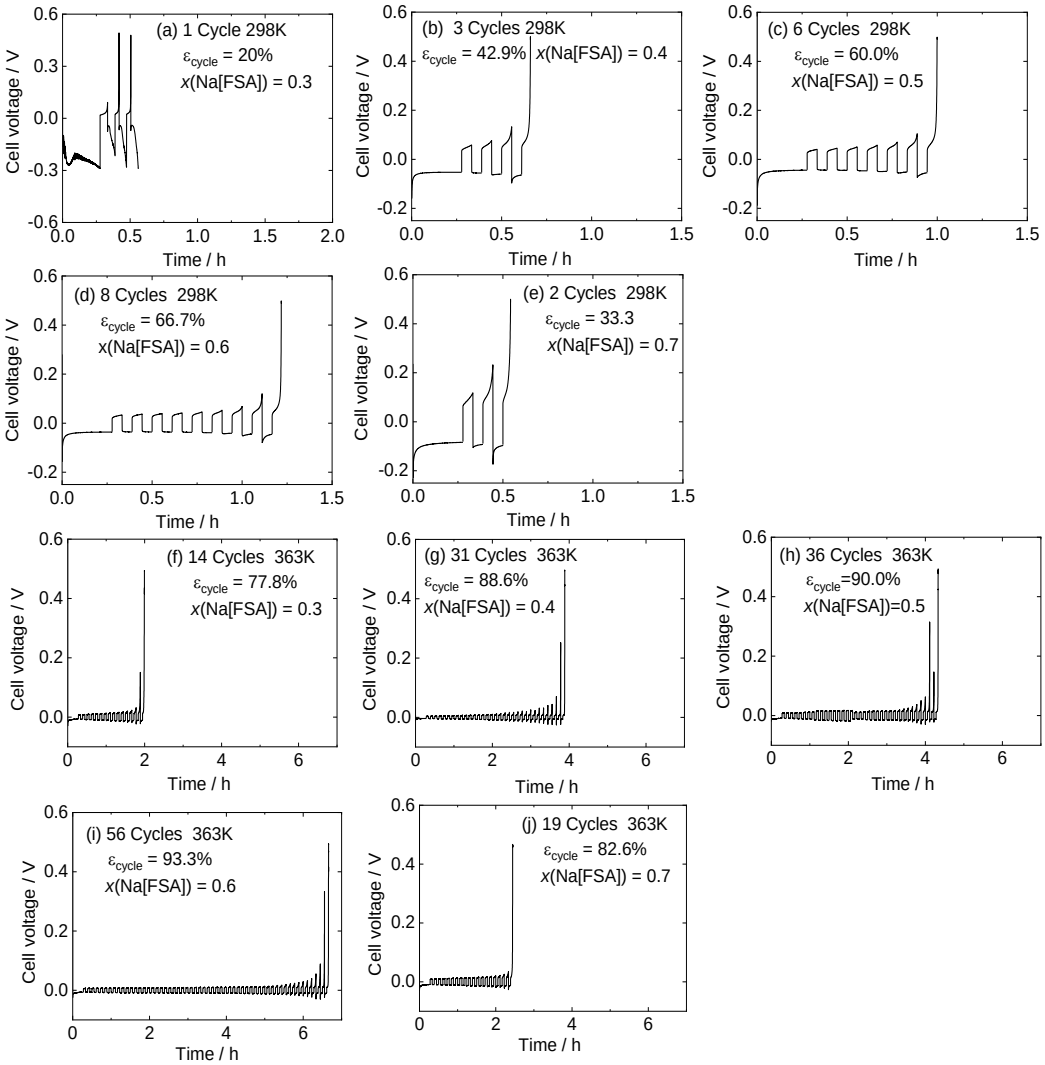


**Figure 7.** Voltage profiles during Na deposition/dissolution in Na[FSA]-[$C_2C_1$pyrr][FSA] at 298 (a–e) and 363 K (f–j) for *x*(Na[FSA]) = 0.3–0.7. The working and counter electrodes were Al and Na plates, respectively. 1 C cm$^{-2}$ Na was deposited on the Al substrate, and 0.2 C cm$^{-2}$ Na deposition and dissolution was repeated until the electrode potential reached 0.5 V vs. $Na^+$/Na during dissolution (see Experimental Section). The current density was ±0.1 mA cm$^{-2}$ for all tests.

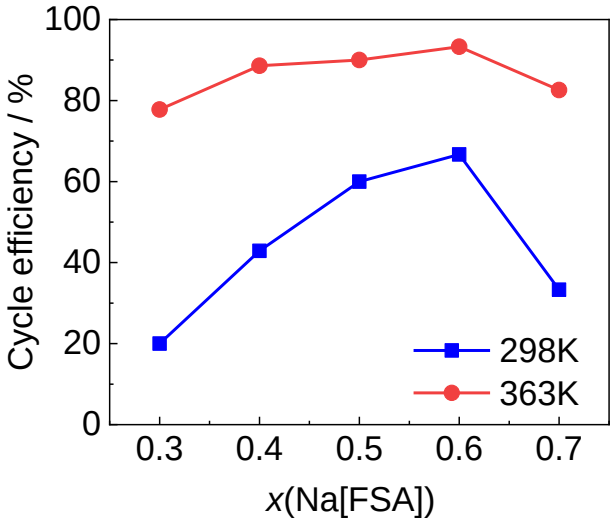


**Figure 8.** Cycle efficiency ($\varepsilon_{cycle}$) of Na metal deposition/dissolution in Na[FSA]-[$C_2C_1$pyrr][FSA] in the range of $x$(Na[FSA]) = 0.3–0.7 at 298 and 363 K.

The suppression of dendritic electrodeposition exceeds electrolyte decomposition at elevated temperatures, which results in a large $\varepsilon_{cycle}$ at 363 K.[56-57] The $\varepsilon_{cycle}$ increases with increasing $x$(Na[FSA]) at 298 and 363 K and reaches a maximum at $x$(Na[FSA]) = 0.6. The formation of SEI is related to the decomposition of electrolyte on Na metal. The SEI film formed by reduction of $FSA^-$–based electrolytes is minimal, which accords with the fact that a high fraction of $Na^+$ in the electrolyte is preferable.[33, 58] Because an increase in $x$(Na[FSA]) provides a stable supply of $Na^+$ at the electrode, the resultant inorganic compound formation is considered to facilitate SEI-layer stabilization and suppresses dendrite formation. Further analytical insights are required to confirm the SEI formation mechanism in the future. A similar interpretation was made in a previous work with a different IL system.[45] The decrease in $\varepsilon_{cycle}$ at $x$(Na[FSA]) = 0.7 likely results from the different properties of SEI layer. This

interpretation is supported by EIS results with symmetric Na/Na cells, which reveal a greater interfacial resistance at this *x*(Na[FSA]) level. The trend of $\varepsilon_{cycle}$ in the deposition/dissolution test is different from that of Coulombic efficiency observed in the cyclic voltammetric tests (Figures 5 and S7). The difference in methodology, which results in the different contact period between the deposited Na metal and electrolyte, probably causes this inconsistency.

3.4. Electrochemical Performance of Na/NVPC cells.

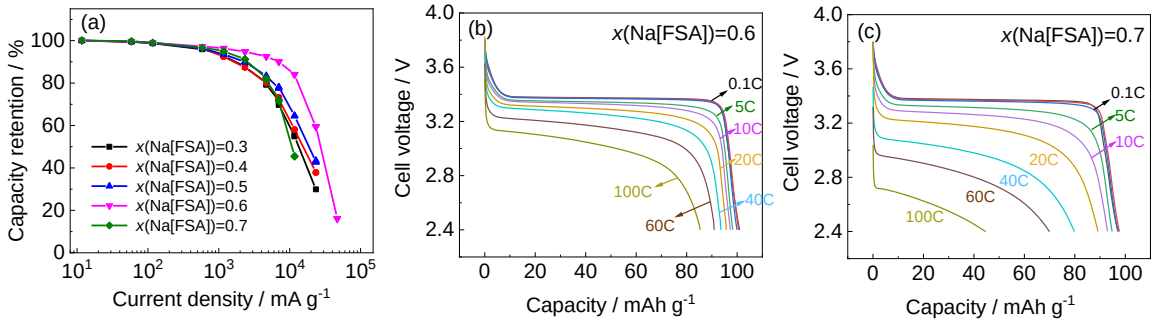


**Figure 9.** Rate capability of Na/NVPC cells at 363 K. (a) Rate capability from 0.1 to 400 C with cutoff voltages of 2.4–3.8 V. (b, c) Discharge curves at *x*(Na[FSA]) = 0.6 and 0.7 from 0.1 to 100 C. Electrolyte: Na[FSA]–[$C_2C_1$pyrr][FSA] (*x*(Na[FSA]) = 0.3–0.7). See Figure S8 for discharge curves at *x*(Na[FSA]) = 0.3–0.5. See Figure S9 for rate capability of Na/NVPC cells at 298 K.

The effect of *x*(Na[FSA]) on the rate capability of the Na[FSA]-[$C_2C_1$pyrr][FSA] system was tested with Na/NVPC cells. The resulting rate capabilities are shown in Figure 9. Figure S9 displays capacities over three cycles as a function of discharge rate at 298 and 363K. Cells were charged galvanostatically at 11.7 mA $g^{-1}$ (0.1 C) and

discharged at current densities from 11.7 mA $g^{-1}$ (0.1 C) to 468000 mA $g^{-1}$ (400 C) (three cycles for each rate) followed by three 0.1 C charge–discharge cycles to confirm retention of the cell. The greatest capacity is observed at $x$(Na[FSA]) = 0.6. The capacity difference among electrolytes with $x$(Na[FSA]) = 0.3–0.7 increases progressively with increasing discharge rate. Discharge curves obtained at 40 C and the corresponding differential capacity vs. voltage plots (d$Q$/d$V$) are shown in Figure S10. Figure S10(a) shows that polarization is greatly alleviated by increasing $x$(Na[FSA]) from 0.3 to 0.6, which highlights the influence of $x$(Na[FSA]) on IL behavior. A similar trend has been observed for the $Na_2FeP_2O_7$ positive electrode in the Na[FSA]-[$C_2C_1$im][FSA] system.[46] The internal resistance, which includes the bulk and interfacial impedance, decreases with increasing Na salt concentration despite the low ionic conductivity present at high $x$(Na[FSA]).[59] Thus, the potential of the reduction peak in the d$Q$/d$V$ plots during discharge moves to more positive values upon increasing $x$(Na[FSA]) from 0.3 to 0.6. At $x$(Na[FSA]) = 0.7, the rate capability diminishes and the peak in the d$Q$/d$V$ plot shifts to a less positive voltage. As encountered in Na metal deposition/dissolution (Figure 7), this behavior results from greater polarization of the Na counter electrode at $x$(Na[FSA]) = 0.7. The capacity retention (0.1C) of all cells after testing is greater than 99% (Figure S9).

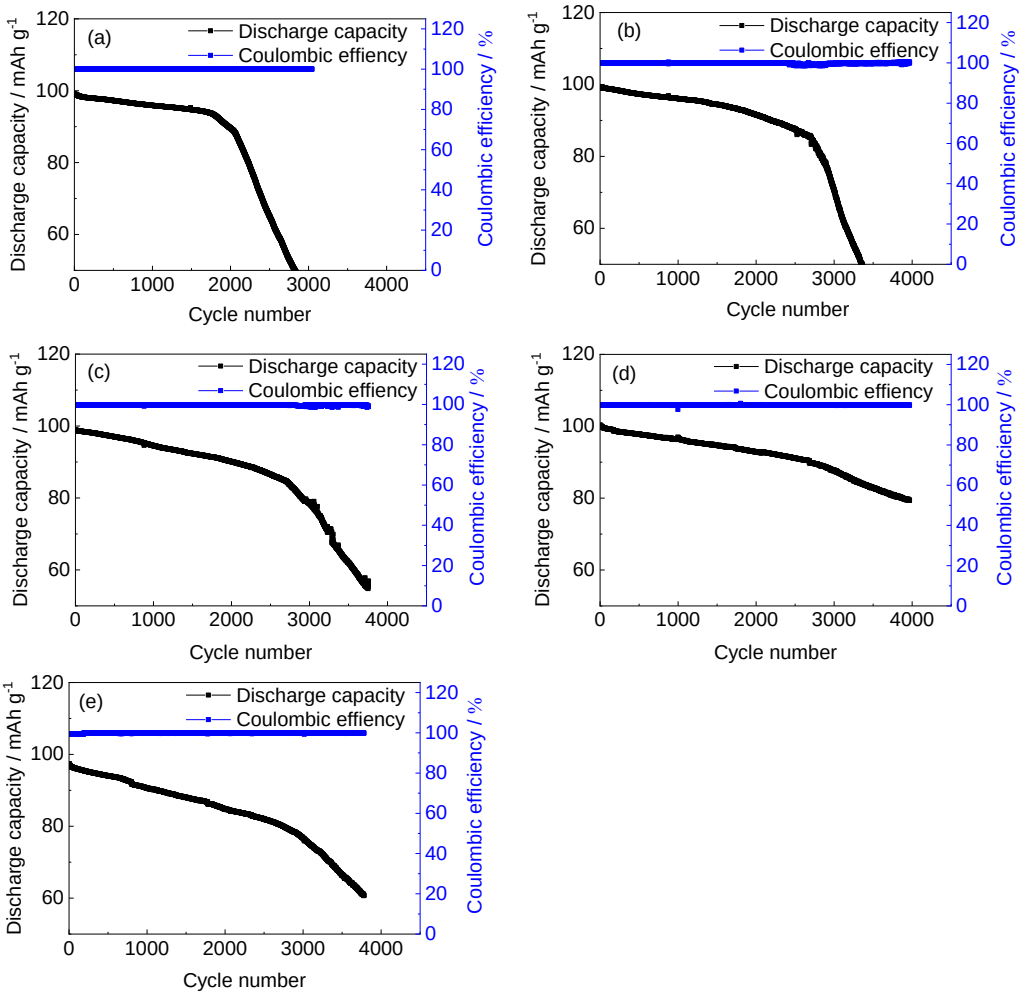


**Figure 10.** Cycling performance of Na/NVPC cells at 363 K. Electrolyte: Na[FSA]–[$C_2C_1$pyrr][FSA] with $x$(Na[FSA]) = 0.3 (a), 0.4 (b), 0.5 (c), 0.6 (d), and 0.7 (e). Charge–discharge rate: 2 C. Cut-off voltages: 2.4–3.8 V. See Figures S11(a) and (b) for discharge curves and corresponding d$Q$/d$V$ plots at 70% capacity retention relative to the first cycle for $x$(Na[FSA]) = 0.3–0.7.

The stable cycling performance of Na/NVPC cells at $x$(Na[FSA]) = 0.3–0.7 and 363 K, which maintain 99.9% efficiency throughout 2000 cycles, is illustrated in Figure 10. The capacity retention increases with increasing $x$(Na[FSA]) until $x$(Na[FSA]) = 0.6, but decreases at $x$(Na[FSA]) = 0.7. Cells with Na[FSA]–[$C_2C_1$pyrr][FSA] electrolyte

containing Na[FSA] ($x$(Na[FSA]) = 0.3–0.7 achieve the capacity retentions of 44.4, 71.2, 79.0, 88.5, and 78.7%, respectively, after 3000 cycles at 2 C. The optimum cycling performance occurs at $x$(Na[FSA]) = 0.6, which provides satisfactory capacity retention (80% retention after 4000 cycles) and high average coulombic efficiency (>99.5%).

3.5. Electrochemical Performance of NVPC/NVPC symmetric cells.

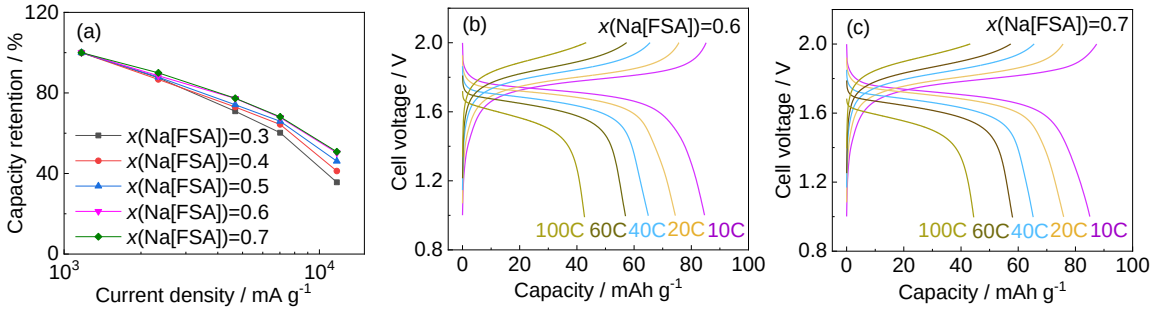


**Figure 11.** Electrochemical measurements of the NVPC/NVPC symmetric cell at 363K. (a) Rate capability from 10 to 100 C at cutoff voltages of 1.0–2.0 V and (b, c) charge–discharge curves at $x$(Na[FSA]) = 0.6 and 0.7. Figure S12 contains charge–discharge curves at $x$(Na[FSA]) = 0.3–0.5.

As shown above and in previous work, Na electrode polarization is significant in IL electrolytes.[46-47] This can be greatly reduced by increasing the operating temperature, but still causes unfavorable effects at high rates. The NVPC/NVPC symmetric cells were assembled to exclude the influence of the Na metal counter electrode in the half-cell and to evaluate the effects of $x$(Na[FSA]) on NVPC electrode performance. The cathode and anode in the NVPC symmetric cell operate via the $V^{3+}/V^{4+}$ and $V^{3+}/V^{2+}$

redox processes described below:[60]

$$\text{(Positive) } Na_3V_2(PO_4)_3 \rightleftarrows NaV_2(PO_4)_3 + 2e^- + 2Na^+ \quad (3)$$

$$\text{(Negative) } Na_3V_2(PO_4)_3 + e^- + Na^+ \rightleftarrows Na_4V_2(PO_4)_3 \quad (4)$$

$$\text{(Total) } 3Na_3V_2(PO_4)_3 \rightleftarrows NaV_2(PO_4)_3 + 2Na_4V_2(PO_4)_3 \quad (5)$$

Although the theoretical capacity ratio of NVPC as positive and negative electrode materials is 2.0:1.0, a 1.0:2.5 mass ratio was used in this study considering their practical capacity values. Figure 11 shows that the rate capability at 363 K increases monotonically with increasing *x*(Na[FSA]) from 0.3 to 0.7. Although the values at *x*(Na[FSA]) = 0.6 and 0.7 are comparable, the discharge capacity at *x*(Na[FSA]) = 0.7 slightly exceeds that at *x*(Na[FSA]) = 0.6. The change of coordination environment as pointed out in the previous work[42] would be one of the factors on this behavior. This clearly demonstrates that the half-cell test using a Na metal counter electrode cannot evaluate the performance of a target material in the present system, and the large Na[FSA] mole fraction provides an advantage in rate capability at 363 K. It should be noticed that the present rate capabilities include the contribution of the $V^{3+}/V^{2+}$ redox activity in addition to the $V^{4+}/V^{3+}$ one. However, they reflect the $V^{4+}/V^{3+}$ contribution more than the case for the Na/NVPC half-cell by considering the smaller $R_{ct}$ of the NVPC/NVPC symmetric cell than that of the Na/Na symmetric cell (see Figure S13, Supporting Information).

## 4. CONCLUSIONS

The thermal, physical, and electrochemical properties of the binary Na[FSA]-[$C_2C_1$pyrr][FSA] system have been investigated. A phase diagram constructed from DSC results reveals that a wide temperature range over 100 K around room temperature is achieved at a broad compositions of $0.3 \leq x$(Na[FSA]) $\leq 0.7$. Valid VTF and Walden plot behavior was established. Sodium deposition/dissolution cycling efficiency increases with increasing temperature and increasing $x$(Na[FSA]) at $0.3 \leq x$(Na[FSA]) $\leq 0.6$. The Na ion concentration in the IL significantly influences the rate and cycle capability of a Na/NVPC half-cell. The optimum electrochemical performance of a Na[FSA]–[$C_2C_1$pyrr][FSA] half-cell operating at 363 K occurs at 60 mol% Na[FSA] and is characterized by superior charge/discharge rates under various operating conditions with good cycling stability over 4000 cycles. NVPC symmetric cell rate tests indicate that the half-cell test is not fully appropriate for evaluating the rate capability of NVPC and that the Na[FSA]–[$C_2C_1$pyrr][FSA] system based on $V^{3+}/V^{4+}$ and $V^{2+}/V^{3+}$ activities improves upon increasing Na[FSA] from 0.3 to 0.7. The high Na ion concentration in the Na[FSA]–[$C_2C_1$pyrr][FSA] system allows the application of this IL electrolyte as high-rate Na secondary batteries especially under an environment with waste heat.

## ASSOCIATED CONTENT

### Supporting Information (PDF)

Supporting Information is available free of charge on the ACS Publications website at

DOI: XXXXXXX.

Synthetic procedure, thermal behavior, viscosity data, ionic conductivity data, detailed discussion of the Walden rule, density data, molar conductivity data, electrochemical measurement data

## AUTHOR INFORMATION

Corresponding Author

E-mail: k-matsumoto@energy.kyoto-u.ac.jp (K.M.).

Notes

The authors declare no competing financial interest.

ORCID

Rika Hagiwara: 0000-0002-7234-3980

Kazuhiko Matsumoto: 0000-0002-0770-9210

Jinkwang Hwang: 0000-0003-4800-3158

## ACKNOWLEDGMENT

This study was partly supported by the Japanese Ministry of Education, Culture, Sports, Science and Technology (MEXT) program “Elements Strategy Initiative to Form Core Research Center” and China Scholarship Council (CSC).

## References

1. Hallett, J. P.; Welton, T., Room-Temperature Ionic Liquids: Solvents for Synthesis and Catalysis. 2. *Chem. Rev.* **2011**, *111*, 3508-3576.

2. Wilkes, J. S., A Short History of Ionic Liquids—from Molten Salts to Neoteric Solvents. *Green Chem* **2002**, *4*, 73-80.

3. Wasserscheid, P.; Keim, W., Ionic Liquids—New "Solutions" for Transition Metal Catalysis. *Angew. Chem. Int. Ed.* **2000**, *39*, 3772-3789.

4. Hagiwara, R.; Ito, Y., Room Temperature Ionic Liquids of Alkylimidazolium Cations and Fluoroanions. *J. Fluorine Chem.* **2000**, *105*, 221-227.

5. Welton, T., Room-Temperature Ionic Liquids. Solvents for Synthesis and Catalysis. *Chem. Rev.* **1999**, *99*, 2071-2084.

6. Hagiwara, R.; Lee, J. S., Ionic Liquids for Electrochemical Devices. *Electrochemistry* **2007**, *75*, 23-34.

7. Ohno, H., *Electrochemical Aspects of Ionic Liquids; John Wiley & Sons*: New York, 2005.

8. Watanabe, M.; Thomas, M. L.; Zhang, S.; Ueno, K.; Yasuda, T.; Dokko, K., Application of Ionic Liquids to Energy Storage and Conversion Materials and Devices. *Chem. Rev.* **2017**, *117*, 7190-7239.

9. Yoo, H. D.; Markevich, E.; Salitra, G.; Sharon, D.; Aurbach, D., On the Challenge of Developing Advanced Technologies for Electrochemical Energy Storage and Conversion. *Mater. Today* **2014**, *17*, 110-121.

10. Béguin, F.; Presser, V.; Balducci, A.; Frackowiak, E., Carbons and Electrolytes for Advanced Supercapacitors. *Adv. Mater.* **2014**, *26*, 2219-2251.

11. MacFarlane, D. R.; Tachikawa, N.; Forsyth, M.; Pringle, J. M.; Howlett, P. C.; Elliott, G. D.; Davis, J. H.; Watanabe, M.; Simon, P.; Angell, C. A., Energy Applications of Ionic Liquids. *Energ. Environ. Sci.* **2014**, *7*, 232-250.

12. Fedorov, M. V.; Kornyshev, A. A., Ionic Liquids at Electrified Interfaces. *Chem. Rev.* **2014**, *114*, 2978-3036.

13. Liu, H.; Liu, Y.; Li, J., Ionic Liquids in Surface Electrochemistry. *Phys. Chem. Chem. Phys.* **2010**, *12*, 1685-1697.

14. Hwang, J.; Matsumoto, K.; Hagiwara, R., $Na_3V_2(PO_4)_3$/C Positive Electrodes with High Energy and Power Densities for Sodium Secondary Batteries with Ionic Liquid Electrolytes That Operate across Wide Temperature Ranges. *Adv. Sustainable Syst.* **2018**, *2*, 1700171.

15. Lin, X.; Salari, M.; Arava, L. M. R.; Ajayan, P. M.; Grinstaff, M. W., High Temperature Electrical Energy Storage: Advances, Challenges, and Frontiers. *Chem. Soc. Rev.* **2016**, *45*, 5848-5887.

16. Canongia Lopes, J. N.; Shimizu, K.; Pádua, A. A.; Umebayashi, Y.; Fukuda, S.; Fujii, K.; Ishiguro, S.-i., Potential Energy Landscape of Bis(Fluorosulfonyl) Amide. *J. Phys. Chem. B* **2008**, *112*, 9449-9455.

17. Xue, L.; Padgett, C. W.; DesMarteau, D. D.; Pennington, W. T., Synthesis and Structures of Alkali Metal Salts of Bis[(Trifluoromethyl)Sulfonyl] Imide. *Solid State Sci.* **2002**, *4*, 1535-1545.

18. Noda, A.; Hayamizu, K.; Watanabe, M., Pulsed-Gradient Spin− Echo $^{1}H$ and $^{19}F$ NMR Ionic Diffusion Coefficient, Viscosity, and Ionic Conductivity of Non-Chloroaluminate Room-Temperature Ionic Liquids. *J. Phys. Chem. B* **2001**, *105*, 4603-4610.

19. Seki, S.; Kihira, N.; Kobayashi, T.; Kobayashi, Y.; Mita, Y.; Takei, K.; Miyashiro, H.; Kuwabata, S., Functionalized Room-Temperature Ionic Liquids for Lithium Secondary Battery Electrolyte Materials. *Electrochemistry* **2009**, *77*, 690-692.

20. Matsumoto, H.; Sakaebe, H.; Tatsumi, K.; Kikuta, M.; Ishiko, E.; Kono, M., Fast Cycling of $Li/LiCoO_2$ Cell with Low-Viscosity Ionic Liquids Based on Bis (Fluorosulfonyl) Imide $[FSI]^-$. *J. Power Sources* **2006**, *160*, 1308-1313.

21. Hayamizu, K.; Tsuzuki, S.; Seki, S.; Fujii, K.; Suenaga, M.; Umebayashi, Y., Studies on the Translational and Rotational Motions of Ionic Liquids Composed of N-Methyl-N-Propyl-Pyrrolidinium ($P_{13}$) Cation and Bis(Trifluoromethanesulfonyl) Amide and Bis(Fluorosulfonyl) Amide Anions and Their

Binary Systems Including Lithium Salts. *J. Chem. Phys.* **2010**, *133*, 194505.
22. Tsunashima, K.; Kawabata, A.; Matsumiya, M.; Kodama, S.; Enomoto, R.; Sugiya, M.; Kunugi, Y., Low Viscous and Highly Conductive Phosphonium Ionic Liquids Based on Bis (Fluorosulfonyl) Amide Anion as Potential Electrolytes. *Electrochem. Commun.* **2011**, *13*, 178-181.
23. Seki, S.; Ohno, Y.; Mita, Y.; Serizawa, N.; Takei, K.; Miyashiro, H., Imidazolium-Based Room-Temperature Ionic Liquid for Lithium Secondary Batteries: Relationships between Lithium Salt Concentration and Battery Performance Characteristics. *ECS Electrochem. Lett.* **2012**, *1*, A77-A79.
24. Shimada, J.; Shimada, M.; Sugahara, T.; Tsunashima, K.; Tani, A.; Tsuchida, Y.; Matsumiya, M., Phase Equilibrium Relations of Semiclathrate Hydrates Based on Tetra-N-Butylphosphonium Formate, Acetate, and Lactate. *J. Chem. Eng. Data* **2018**, *63*, 3615-3620.
25. Best, A.; Bhatt, A.; Hollenkamp, A., Ionic Liquids with the Bis (Fluorosulfonyl) Imide Anion: Electrochemical Properties and Applications in Battery Technology. *J. Electrochem. Soc.* **2010**, *157*, A903-A911.
26. Yoon, H.; Howlett, P.; Best, A.; Forsyth, M.; MacFarlane, D., Fast Charge/Discharge of Li Metal Batteries Using an Ionic Liquid Electrolyte. *J. Electrochem. Soc.* **2013**, *160*, A1629-A1637.
27. Bhatt, A. I.; Kao, P.; Best, A. S.; Hollenkamp, A. F., Understanding the Morphological Changes of Lithium Surfaces During Cycling in Electrolyte Solutions of Lithium Salts in an Ionic Liquid. *J. Electrochem. Soc.* **2013**, *160*, A1171-A1180.
28. Borodin, O.; Gorecki, W.; Smith, G. D.; Armand, M., Molecular Dynamics Simulation and Pulsed-Field Gradient NMR Studies of Bis(Fluorosulfonyl) Imide (FSI) and Bis[(Trifluoromethyl) Sulfonyl] Imide(TFSI)-Based Ionic Liquids. *J. Phys. Chem. B* **2010**, *114*, 6786-6798.
29. Budi, A.; Basile, A.; Opletal, G.; Hollenkamp, A. F.; Best, A. S.; Rees, R. J.; Bhatt, A. I.; O'Mullane, A. P.; Russo, S. P., Study of the Initial Stage of Solid Electrolyte Interphase Formation Upon Chemical Reaction of Lithium Metal and N-Methyl-N-Propyl-Pyrrolidinium-Bis (Fluorosulfonyl) Imide. *J. Phys. Chem. C* **2012**, *116*, 19789-19797.
30. Zakeeruddin, S. M.; Grätzel, M., Solvent-Free Ionic Liquid Electrolytes for Mesoscopic Dye-Sensitized Solar Cells. *Adv. Funct. Mater.* **2009**, *19*, 2187-2202.
31. Han, H.-B.; Zhou, S.-S.; Zhang, D.-J.; Feng, S.-W.; Li, L.-F.; Liu, K.; Feng, W.-F.; Nie, J.; Li, H.; Huang, X.-J., Lithium Bis(Fluorosulfonyl) Imide (LiFSI) as Conducting Salt for Nonaqueous Liquid Electrolytes for Lithium-Ion Batteries: Physicochemical and Electrochemical Properties. *J. Power Sources* **2011**, *196*, 3623-3632.
32. Xu, W.; Wang, J.; Ding, F.; Chen, X.; Nasybulin, E.; Zhang, Y.; Zhang, J.-G., Lithium Metal Anodes for Rechargeable Batteries. *Energ. Environ. Sci.* **2014**, *7*, 513-537.
33. Shkrob, I. A.; Marin, T. W.; Zhu, Y.; Abraham, D. P., Why Bis (Fluorosulfonyl) Imide Is a "Magic Anion" for Electrochemistry. *J. Phys. Chem. C* **2014**, *118*, 19661-19671.
34. Basile, A.; Hollenkamp, A. F.; Bhatt, A. I.; O'Mullane, A. P., Extensive Charge–Discharge Cycling of Lithium Metal Electrodes Achieved Using Ionic Liquid Electrolytes. *Electrochem. Commun.* **2013**, *27*, 69-72.
35. Ishikawa, M.; Sugimoto, T.; Kikuta, M.; Ishiko, E.; Kono, M., Pure Ionic Liquid Electrolytes Compatible with a Graphitized Carbon Negative Electrode in Rechargeable Lithium-Ion Batteries. *J. Power Sources* **2006**, *162*, 658-662.
36. Schweikert, N.; Hofmann, A.; Schulz, M.; Scheuermann, M.; Boles, S. T.; Hanemann, T.; Hahn, H.; Indris, S., Suppressed Lithium Dendrite Growth in Lithium Batteries Using Ionic Liquid Electrolytes: Investigation by Electrochemical Impedance Spectroscopy, Scanning Electron Microscopy, and in Situ

$^{7}$Li Nuclear Magnetic Resonance Spectroscopy. *J. Power Sources* **2013**, *228*, 237-243.

37. Tarascon, J.-M., Is Lithium the New Gold? *Nat. Chem.* **2010**, *2*, 510.

38. Hwang, J.-Y.; Myung, S.-T.; Sun, Y.-K., Sodium-Ion Batteries: Present and Future. *Chem. Soc. Rev.* **2017**, *46*, 3529-3614.

39. Yabuuchi, N.; Kubota, K.; Dahbi, M.; Komaba, S., Research Development on Sodium-Ion Batteries. *Chem. Rev.* **2014**, *114*, 11636-11682.

40. Matsumoto, K.; Hosokawa, T.; Nohira, T.; Hagiwara, R.; Fukunaga, A.; Numata, K.; Itani, E.; Sakai, S.; Nitta, K.; Inazawa, S., The Na [FSA]–[$C_2C_1$im][FSA]($C_2C_1im^+$:1-ethyl-3-methylimidazolium and $Fsa^-$: Bis (Fluorosulfonyl) Amide) Ionic Liquid Electrolytes for Sodium Secondary Batteries. *J. Power Sources* **2014**, *265*, 36-39.

41. Matsumoto, K.; Okamoto, Y.; Nohira, T.; Hagiwara, R., Thermal and Transport Properties of Na[N($SO_2F)_2$]–[N-Methyl-N-propylpyrrolidinium][N($SO_2F)_2$] Ionic Liquids for Na Secondary Batteries. *J. Phys. Chem. C* **2015**, *119*, 7648-7655.

42. Forsyth, M.; Yoon, H.; Chen, F.; Zhu, H.; MacFarlane, D. R.; Armand, M.; Howlett, P. C., Novel $Na^+$ Ion Diffusion Mechanism in Mixed Organic–Inorganic Ionic Liquid Electrolyte Leading to High $Na^+$ Transference Number and Stable, High Rate Electrochemical Cycling of Sodium Cells. *J. Phys. Chem. C* **2016**, *120*, 4276-4286.

43. Ding, C.; Nohira, T.; Hagiwara, R.; Matsumoto, K.; Okamoto, Y.; Fukunaga, A.; Sakai, S.; Nitta, K.; Inazawa, S., Na[FSA]-[$C_3C_1$pyrr][FSA] Ionic Liquids as Electrolytes for Sodium Secondary Batteries: Effects of Na Ion Concentration and Operation Temperature. *J. Power Sources* **2014**, *269*, 124-128.

44. Basile, A.; Hilder, M.; Makhlooghiazad, F.; Pozo‐Gonzalo, C.; MacFarlane, D. R.; Howlett, P. C.; Forsyth, M., Ionic Liquids and Organic Ionic Plastic Crystals: Advanced Electrolytes for Safer High Performance Sodium Energy Storage Technologies. *Adv. Energy Mater.* **2018**, *8*, 1703491.

45. Hilder, M.; Howlett, P. C.; Saurel, D.; Gonzalo, E.; Basile, A.; Armand, M.; Rojo, T.; Kar, M.; MacFarlane, D. R.; Forsyth, M. The Effect of Cation Chemistry on Physicochemical Behaviour of Superconcentrated Nafsi Based Ionic Liquid Electrolytes and the Implications for Na Battery Performance. *Electrochim. Acta* **2018**, *268*, 94-100.

46. Hwang, J.; Matsumoto, K.; Hagiwara, R., Symmetric Cell Electrochemical Impedance Spectroscopy of $Na_2FeP_2O_7$ Positive Electrode Material in Ionic Liquid Electrolytes. *J. Phys. Chem. C* **2018,** 122, 26857−26864.

47. Wang, C.-H.; Yang, C.-H.; Chang, J.-K., Suitability of Ionic Liquid Electrolytes for Room-Temperature Sodium-Ion Battery Applications. *Chem. Commun.* **2016**, *52*, 10890-10893.

48. Yoshizawa-Fujita, M.; Kishi, E.; Suematsu, M.; Takekawa, T.; Rikukawa, M., A Plastic Electrolyte Material in a Highly Desirable Temperature Range: N-Ethyl-N-methylpyrrolidinium Bis(fluorosulfonyl) amide. *Chem. Lett.* **2014**, *43*, 1909-1911.

49. Jian, Z.; Yuan, C.; Han, W.; Lu, X.; Gu, L.; Xi, X.; Hu, Y. S.; Li, H.; Chen, W.; Chen, D., Atomic Structure and Kinetics of NASICON $Na_xV_2(PO_4)_3$ Cathode for Sodium-Ion Batteries. *Adv. Funct. Mater.* **2014**, *24*, 4265-4272.

50. Jian, Z.; Zhao, L.; Pan, H.; Hu, Y.-S.; Li, H.; Chen, W.; Chen, L., Carbon Coated $Na_3V_2(PO_4)_3$ as Novel Electrode Material for Sodium Ion Batteries. *Electrochem. Commun.* **2012**, *14*, 86-89.

51. Kubota, K.; Nohira, T.; Goto, T.; Hagiwara, R., Novel Inorganic Ionic Liquids Possessing Low Melting Temperatures and Wide Electrochemical Windows: Binary Mixtures of Alkali Bis (Fluorosulfonyl) Amides. *Electrochem. Commun.* **2008**, *10*, 1886-1888.

52. Hirao, M.; Sugimoto, H.; Ohno, H., Preparation of Novel Room-Temperature Molten Salts by Neutralization of Amines. *J. Electrochem. Soc.* **2000**, *147*, 4168-4172.

53. Matsumoto, K.; Oka, T.; Nohira, T.; Hagiwara, R., Polymorphism of Alkali Bis(fluorosulfonyl) amides (M[$N(SO_2F)_2$], M= Na, K, and Cs). *Inorg. Chem.* **2012**, *52*, 568-576.

54. Matsumoto, K.; Nishiwaki, E.; Hosokawa, T.; Tawa, S.; Nohira, T.; Hagiwara, R., Thermal, Physical, and Electrochemical Properties of Li[$N(SO_2F)_2$]-[1-Ethyl-3-methylimidazolium][$N(SO_2F)_2$] Ionic Liquid Electrolytes for Li Secondary Batteries Operated at Room and Intermediate Temperatures. *J. Phys. Chem. C* **2017**, *121*, 9209-9219.

55. Liu, K.; Zhou, Y.-X.; Han, H.-B.; Zhou, S.-S.; Feng, W.-F.; Nie, J.; Li, H.; Huang, X.-J.; Armand, M.; Zhou, Z.-B., Ionic Liquids Based on (fluorosulfonyl)(pentafluoroethanesulfonyl)imide with Various Oniums. *Electrochim. Acta* **2010**, *55*, 7145-7151.

56. Matsumoto, K.; Taniki, R.; Nohira, T.; Hagiwara, R., Inorganic–Organic Hybrid Ionic Liquid Electrolytes for Na Secondary Batteries. *J. Electrochem. Soc.* **2015**, *162*, A1409-A1414.

57. T. Nohira, T. H., Kazuhiko Matsumoto, Rika Hagiwara, Deposition-Dissolution Behavior and Possibility of Suppression of Dendrite Growth for Sodium Metal in Ionic Liquids. *Denki Kagaku* **2018**, *86*, 293-297.

58. Hosokawa, T.; Matsumoto, K.; Nohira, T.; Hagiwara, R.; Fukunaga, A.; Sakai, S.; Nitta, K., Stability of Ionic Liquids against Sodium Metal: A Comparative Study of 1-Ethyl-3-methylimidazolium Ionic Liquids with Bis(fluorosulfonyl)amide and Bis(trifluoromethylsulfonyl)amide. *J. Phys. Chem. C* **2016**, *120*, 9628-9636.

59. Chen, C.-Y.; Kiko, T.; Hosokawa, T.; Matsumoto, K.; Nohira, T.; Hagiwara, R., Ionic Liquid Electrolytes with High Sodium Ion Fraction for High-Rate and Long-Life Sodium Secondary Batteries. *J. Power Sources* **2016**, *332*, 51-59.

60. Plashnitsa, L. S.; Kobayashi, E.; Noguchi, Y.; Okada, S.; Yamaki, J.-i., Performance of NASICON Symmetric Cell with Ionic Liquid Electrolyte. *J. Electrochem. Soc.* **2010**, *157*, A536-A543.

TOC Graphic

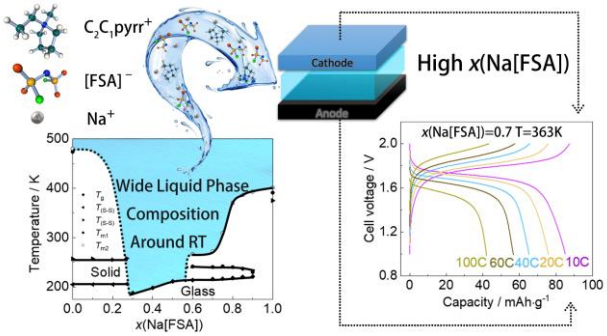
C2C1pyrr+
[FSA] −
Na+
Cathode
Anode
High x(Na[FSA])
Wide Liquid Phase
Composition
Around RT
Solid
Glass
Temperature / K
x(Na[FSA])
x(Na[FSA])=0.7 T=363K
Cell voltage / V
Capacity / mAh·g-1
100C 60C 40C 20C 10C